Ocean Engineering 38 (2011) 2077–2088

Contents lists available at SciVerse ScienceDirect

Ocean Engineering

journal homepage: www.elsevier.com/locate/oceaneng

Models for pollutant behavior in Spanish–Moroccan waters

R. Periáñez *

Dpto. Física Aplicada I, ETSIA, Universidad de Sevilla, Ctra. Utrera km 1, 41013 Sevilla, Spain

ARTICLE INFO

Article history:
Received 1 July 2011
Accepted 10 September 2011
Editor-in-Chief: A.I. Incecik
Available online 25 September 2011

Keywords:
Numerical modelling
Dispersion
Alboran Sea
Gulf of Cadiz
Plutonium
Caesium
Heavy metals
Oil spills

ABSTRACT

The dispersion of pollutants in the Alboran Sea and the Gulf of Cadiz has been studied using numerical models. Two types of dispersion models have been developed: finite difference and particle-tracking ones. In both cases, water currents are obtained from hydrodynamic models suited for each domain. Thus, a 2-layer model is adopted for the Alboran Sea and a 3D baroclinic model for the Gulf of Cadiz. Hydrodynamic models have been tested through comparisons of computed tides and currents with measurements in the regions. Finite difference dispersion models include water–sediment interactions and are applied to simulate the dispersion of heavy metals and fallout radionuclides in the Gulf of Cadiz and Alboran Sea, respectively. Comparisons of computed metal and radionuclide concentrations, in bed sediments and the water column, with measurements provide an extra validation of the hydrodynamics. Particle-tracking rapid-response models are described for each region and some applications cases are presented. These models allow an extremely fast assessment of the consequences of an accidental or deliberate release of pollutants at any depth in the water column. Also, they may provide useful information, through numerical experiments, about oceanographic processes occurring in the area, for instance mixing processes.

1. Introduction

The Gulf of Cadiz (GoC) and the Alboran Sea (AS) connect the Atlantic Ocean and the Mediterranean Sea through the Strait of Gibraltar (see Fig. 1). The GoC is responsible for 5–10% of fish and shell-fish catches of Spain and Portugal holding important living resources of commercial and ecological interest (Beckers et al., 2007). Similarly, the AS is one of the most productive areas in the Mediterranean (Masqué et al., 2003). Consequently, it is relevant to study and understand the geochemistry and dispersion patterns of pollutants in the GoC and AS systems, since this will help assessing the potential influence of contaminants on ecosystem functioning.

The objective of this work consists of describing pollutant dispersion models developed for the AS and GoC. Dispersion models are based upon appropriate hydrodynamic models which provide water circulation in each system. The hydrodynamic descriptions are validated through the comparison of measured and computed tides and currents. Further validation is obtained by applying the computed hydrodynamic to simulate the dispersion of fallout radionuclides (^{137}Cs and ^{239,240}Pu) in the AS and of heavy metals (Zn and Cu) in the GoC. These metals are introduced by three rivers (Guadiana, Odiel-Tinto and Guadalquivir) draining a large mining area (the Iberian Pyrite Belt) in the southern Iberian Peninsula (Sainz and Ruiz, 2006). These radionuclides and metals have been considered since there are enough experimental data on their environmental concentrations which can be used to test the models. Computed metal and radionuclide concentrations in the water column and in bed sediments have been compared with measurements carried out in both domains. Consequently, these dispersion models include water–sediment interactions, which are described in a dynamic way through kinetic transfer coefficients. Finally, 3D rapid-response Lagrangian models for the AS and GoC are constructed over the same hydrodynamics as the finite difference models. These models allow an extremely fast assessment of the consequences of an accidental or deliberate release of pollutants in the water column. This is a relevant issue since, for instance, there is an intense traffic of nuclear submarines and oil tankers through the Strait of Gibraltar.

Thus, two types of dispersion models have been developed: finite-difference models including water–sediment interactions and Lagrangian (or particle-tracking) models for dissolved pollutants and oil spills. The first type is useful to provide an insight of the main environmental and transport processes in the GoC and AS and may be applied, for instance, to predict the effects of planned routine releases in the systems. The second type is a predictive tool which may be used to support the decision-making process after an emergency.

In any case, a detailed knowledge of the hydrodynamics of each system is required. A brief description of the hydrodynamic

* Tel.: +34 954486474; fax: +34 954486436.
E-mail address: rperianez@us.es

0029-8018/$ - see front matter © 2011 Elsevier Ltd. All rights reserved.
doi:10.1016/j.oceaneng.2011.09.005

models is given in the following section. Next, finite-difference dispersion models are presented. Finally, the Lagrangian models are described and some application examples provided.

2. Hydrodynamic models

2.1. Model descriptions

The water current at any position is obtained through the addition of the instantaneous barotropic tidal current plus a residual (mean or long-term) circulation. Both in the GoC and the AS, tides are computed using a 2D depth-averaged model, which is a reasonable approach (Dyke, 2001; Yanagi, 1999) already used successfully in the Strait of Gibraltar (Periáñez and Pascual-Granged, 2008). Tidal equations are standard and may be seen, for instance, in Periáñez (2005a). The solution of these equations provides the water currents at each point in the model domain and for each time step. Currents are treated through standard tidal analysis (Pugh, 1987) and tidal

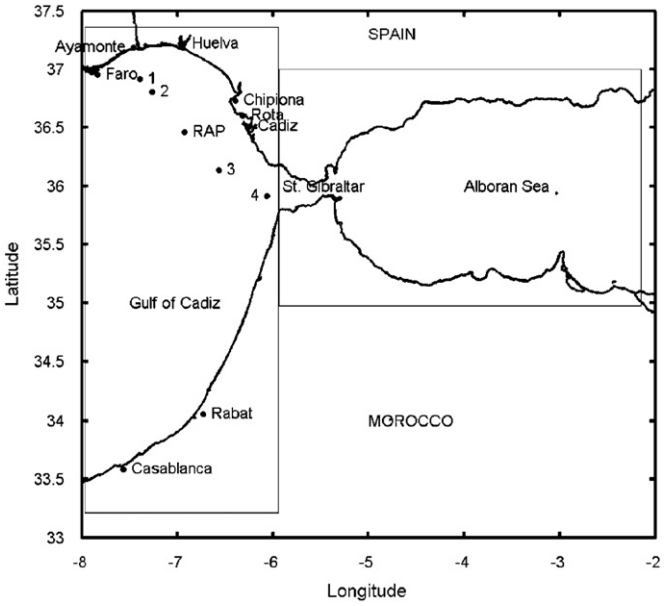

Fig. 1. Map of the GoC and AS showing all locations mentioned in the text. The domains of both models are indicated by the rectangular boxes. The mouths of the Guadiana, Odiel-Tinto and Guadalquivir rivers, in the GoC, are located in Ayamonte, Huelva and Chipiona, respectively.

constants are stored in files that will be read by the transport models. The two main tidal constituents, M_2 and S_2, are considered. Thus, the hydrodynamic equations are solved for each constituent and tidal analysis is also carried out for each constituent separately. Tidal constants allow a very fast calculation of the tidal current at any time and point in the domain. Diurnal constituents are not included since most of the variance of current velocities is given by the M_2 signal alone, S_2 being the second important constituent. Therefore they can be used to characterize a very significant fraction of tides in the areas (Mañanes et al., 1998).

From an operative point of view, circulation in the Strait of Gibraltar and the AS may be simplified to a 2-layer system with water flowing in opposite directions: an upper layer of Atlantic Water flowing to the east, and a more dense bottom layer flowing to the west (Echevarría et al., 2002). This approach has already been used to study the water exchanges between the Atlantic and the Mediterranean by means of numerical models (Izquierdo et al., 2001; Heburn and La Violette, 1990). Consequently, a 2-layer model has been adopted to calculate the residual circulation in the AS. Equations may be seen in the above mentioned references.

Complex mixing processes between several water masses occur in the GoC (Criado-Aldeanueva et al., 2006), thus a full 3D primitive-equation baroclinic hydrodynamic model is used. It is based upon the hydrostatic and Boussinesq approximations on a β plane. The model includes equations for salinity and temperature evolution and water density is calculated from them using a standard state equation. A 1-equation turbulence model has been used to calculate the vertical eddy viscosity. Details on the 3D equations may be seen, for instance, in Kowalick and Murty (1993). A summary of the main characteristics of hydrodynamic models may be seen in Table 1.

Residual circulations in the GoC and AS are again stored in files which are appropriately read by the dispersion codes. A summary of equations involved in the different hydrodynamic models may be seen in Appendix A.

2.2. Results

Equations in all models are solved using finite difference schemes with appropriate boundary conditions (Table 1). Domains of the GoC and AS models are shown as rectangular boxes in Fig. 1. Spatial resolution of the grid is 2 min in longitude and latitude for both domains, and time step in each model is selected carefully to satisfy all stability conditions. Seabed topography has been obtained from the NOAA (US National Ocean and Atmosphere Administration)

Table 1
Summary of hydrodynamic model characteristics.

	2D model	2-Layer model	3D model
Domain	GoC, AS	AS	GoC
Objective	Tides	Mean circulation	Mean circulation
Spatial resolution	2 min[a]	2 min[a]	2 min[a]
Features	Barotropic depth-averaged. M_2, S_2 constituents, tidal analysis	2 water layers with constant density	Hydrostatic, Boussinesq baroclinic equations for T and S. 1-equation turbulence model
Forcing	Tide amplitude and phase along open boundaries	Water exchanges through Gibraltar Strait	Water exchanges through Gibraltar Strait and T, S from climatology
Forcing data source	Schwiderski (1980a, 1980b) and Tsimplis et al. (1995)	Preller (1986)	Preller (1986), WOA05 climatology[b]
Additional boundary condition where required	Radiation[c]	Radiation[c]	Radiation[c]

[a] In both longitude and latitude.
[b] World Ocean Atlas 2005, National Ocean and Atmosphere Administration, available on-line. Seasonal values have been used.
[c] See Mellor (2004).

GEODAS database, available on-line. In the case of the 3D model of the GoC, 50 vertical levels are used.

A detailed comparison of results of the tidal model with measurements in the AS is given in Periáñez (2006) and will not be repeated here. In the case of the GoC, a comparison of computed and measured tide amplitudes and phases at several locations is presented in Table 2. The amplitude of the tide is about 1 m over all the GoC, decreasing near the Strait of Gibraltar. Associated currents are weak with amplitudes below 0.10 m/s over most of the GoC. Indeed at the RAP (Red de Aguas Profundas, Spanish Institute of Oceanography) buoy position (see Fig. 1), the M_2 barotropic tidal current is less than 0.03 m/s (García-Lafuente et al., 2006). The computed current at this position is 0.034 m/s. The current amplitude increases on approaching the Strait entrance, where currents about 0.8 m/s are observed.

Table 2
Established, index *obs* (NOAA, 1982) and computed, index *comp*, amplitudes (A, cm) and phases (g, deg) of tidal elevations at several locations indicated in Fig. 1.

Station	M_2				S_2			
	A_{obs}	g_{obs}	A_{comp}	g_{comp}	A_{obs}	g_{obs}	A_{comp}	g_{comp}
Faro	92	94	99	68	32	125	36	91
Chipiona	102	54	104	62	41	82	38	85
Rota	105	52	103	62	37	78	38	85
Cadiz	100	87	99	61	37	110	36	83
Ayamonte	100	59	101	65	32	88	36	89
Huelva	102	56	105	65	38	82	38	88
Casablanca	99	56	92	53	35	81	36	77
Rabat	88	59	98	57	35	83	36	78

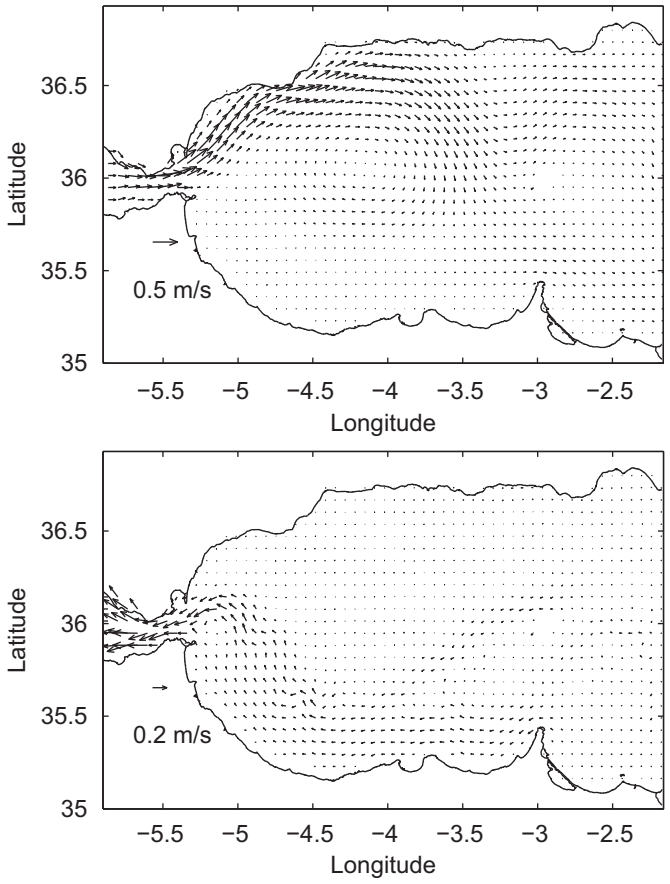

Fig. 2. Computed residual currents in the upper (up) and lower (down) water layers of the AS. Only one of each four computed vectors is shown for clarity.

The residual circulation in the AS, in both water layers, is shown in Fig. 2. A large anticyclonic eddy, known as WAG (Western Alboran Gyre), is observed. This is an almost permanent feature of surface circulation in the AS (Perkins et al., 1990). A detailed description, together with comparisons of model results with measurements, is given in Periáñez (2008).

The residual surface circulation in the northern GoC is characterized by a current directed to the SE (Criado-Aldeanueva et al., 2006) along the Spanish coast. This circulation is a rather constant pattern during most of the year. Part of the flow enters the Strait of Gibraltar and part is deflected to the south. The summer residual circulation computed with the baroclinic model at the sea surface is presented in Fig. 3 as an example. The current is effectively directed to the SE over the Spanish continental shelf and part of this flow enters the Strait of Gibraltar. Maximum currents are of the order of 0.3 m/s in agreement with García-Lafuente et al. (2006). The anticyclonic eddy at the east of Faro (see Fig. 1) has been described by Machín et al. (2006). Also, the cyclonic eddy in front of the Strait of Gibraltar also appears clearly in the models of Beckers et al. (2007) and Peliz et al. (2007).

Below the surface, the Mediterranean waters flow into the Atlantic and mainly to the NW (Ambar and Howe, 1979). As an example, the computed circulation 590 m below the surface is presented in Fig. 4. Only the northern part of the GoC is shown to appreciate details more clearly. This current field is in agreement

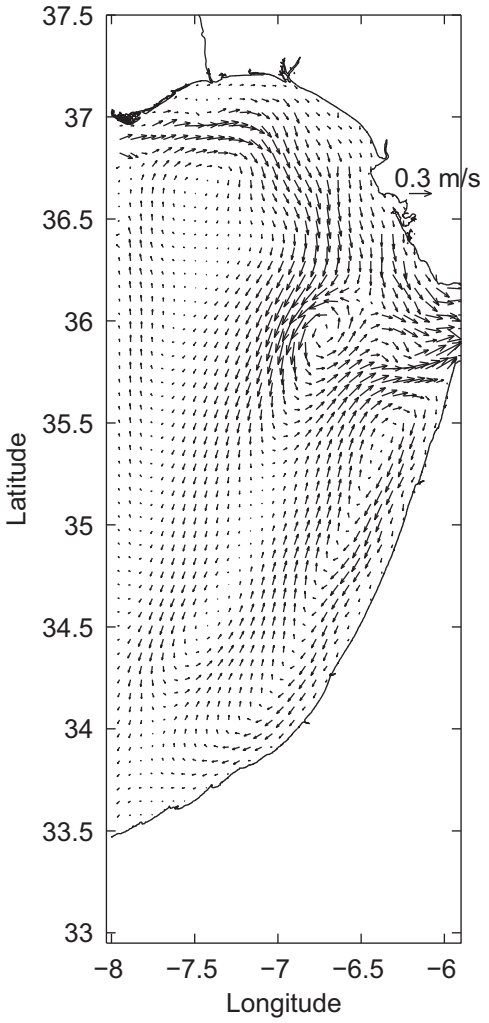

Fig. 3. Computed surface residual currents in the GoC. Only one of each four vectors is drawn.

with Criado-Aldeanueva et al. (2006). Water velocity is higher close to the Strait and then slows to about 0.1 m/s in agreement with Ambar and Howe (1979).

Temperature and salinity profiles in the water column, calculated by the model using summer climatology data for forcing, have been compared with those obtained from observations carried out under the TOROS project (Elbaz-Poulichet et al., 2001) in summer 1997.

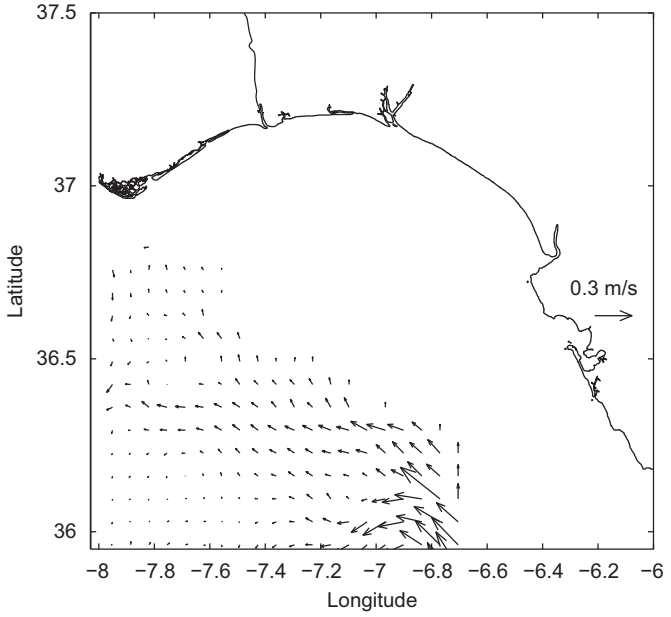

Fig. 4. Computed residual currents 590 m below the surface in the northern GoC. Only one of each four vectors is drawn.

Examples for four points shown in Fig. 1 may be seen in Fig. 5. There is an acceptable agreement between model results and experimentally obtained vertical profiles of *T* and *S*.

3. Finite difference dispersion models

3.1. Description

Finite-difference dispersion models consist of an advection–diffusion equation with added terms, which describe pollutant exchanges between the liquid and solid (suspended matter and bed sediment) phases. These adsorption/release reactions are described by means of kinetic transfer coefficients (Periáñez, 2005a). A sediment transport model is also required to obtain suspended matter concentrations and sedimentation rates. Sediment transport is described by an advection–diffusion equation to which some terms are added. These are external sources of particles, terms describing particle deposition on the seabed and erosion from the bed to the water column, and vertical settling. The formulation of these processes is based upon standard formulae (Periáñez, 2005b; Lumborg and Windelin, 2003; Cancino and Neves, 1999). Suspended sediment equations in a 3D formulation are summarized in Appendix B.

The descriptions of sediment and pollutant transport have been adapted to a 2-layered sea and applied to the Alboran Sea (Periáñez, 2008). Non-conservative pollutants are those which do not remain dissolved in the water column but have a certain affinity to be fixed to particles. If the contaminant is introduced in the surface water layer, it will be fixed to settling suspended particles and their deposition on the seabed will contaminate the bottom sediment. Of course there are also advection/diffusion processes in both water layers, diffusion of dissolved contaminants and of suspended matter particles through the pycnocline and direct adsorption of pollutants

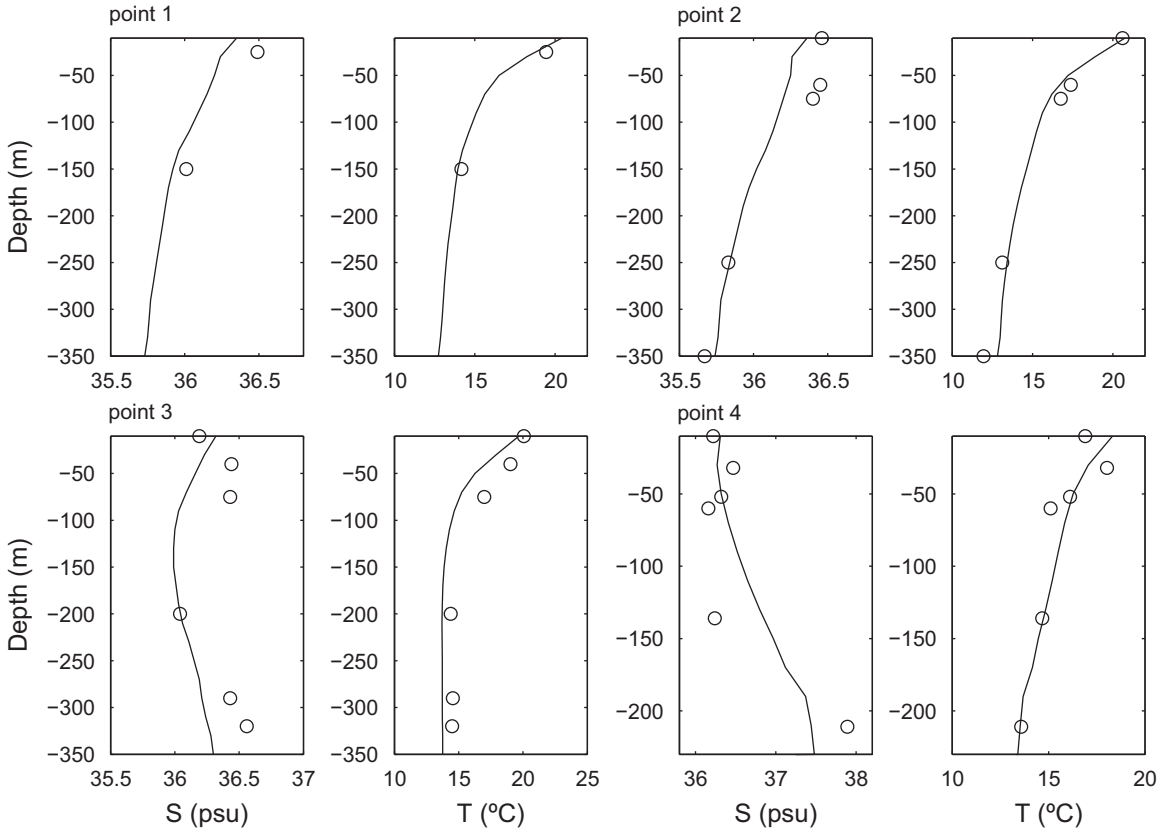

Fig. 5. Computed (lines) and measured (points) salinity and temperature profiles in points indicated in Fig. 1.

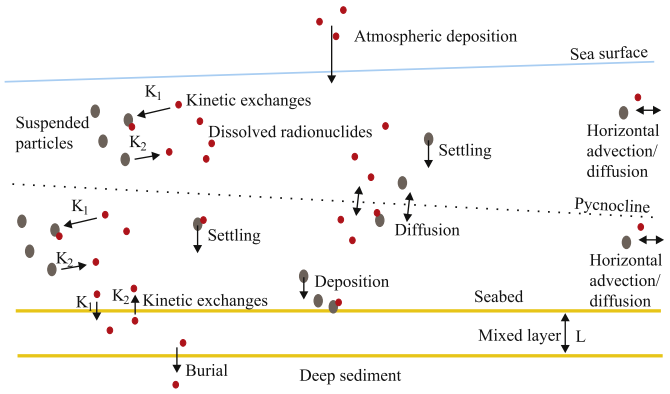

Fig. 6. Processes affecting the dispersion of non-conservative pollutants in a 2-layer sea. Black circles are suspended sediment particles and the red ones are contaminant particles. (For interpretation of the references to color in this figure legend, the reader is referred to the web version of this article.)

on the seabed. The exchanges between the dissolved and solid phases may be described in terms of kinetic transfer coefficients. Thus, assuming that adsorption/release reactions are governed by a single reversible reaction, a coefficient k_1 governs the transfer from the liquid to the solid phase and a coefficient k_2 governs the inverse process. Also, the migration of pollutants to the deep sediment must be included since simulations over several years are carried out. Thus, pollutants deposited on the sediment surface will be buried by particle deposition and will migrate below the mixed sediment layer that directly interacts with the dissolved phase. A summary of all the processes involved (in a 2-layer approach) may be seen in Fig. 6.

Transport equations in a 3D form, including kinetic processes, may be seen in Periáñez (2004). Processes are the same as described above and presented in Fig. 6. Main equations are summarized in Appendix C in the case of a 2-layer sea. They are easily converted into a 3D form.

3.2. Results

Finite difference dispersion models have been applied to simulate the transport of heavy metals in the GoC and of fallout radionuclides in the AS, as has been commented before.

Computed ^{137}Cs and ^{239,240}Pu concentrations, introduced from fallout, in the water column at different depths and in bed sediments have been compared with observations in the AS. Computed radionuclide fluxes through the Strait of Gibraltar have been compared with previous estimates as well. All these results have already been published (Periáñez, 2008) and are not repeated here. However, as an example, the computed ^{137}Cs concentrations corresponding to unfiltered water for both water layers are presented in Fig. 7. The distribution in the upper layer shows higher concentrations in the area occupied by the WAG. This is due to the fact that some water is trapped in the gyre and thus its radionuclide concentration increases as a result of the atmospheric input. Nevertheless, simulations are made under steady flow conditions, thus this pattern will be destroyed by episodes of migration and disappearance of the WAG and winds. However, it is worth commenting that the pattern of higher radionuclide concentrations (for ^{210}Pb, introduced by atmospheric deposition as well) in the centre of the oceanic gyres (in both the Pacific and North Atlantic) has already been detected (Ivanovich and Harmon, 1992, page 384). Consequently, the radionuclide enhancement in the WAG is a real process, although overestimated because of the simulation conditions (steady residual flow). ^{137}Cs distribution is rather uniform in the deep water layer.

Three-dimensional transport equations have been used to simulate Cu and Zn dispersion in the GoC. Published models describing trace metal dispersion in the GoC consider metals as

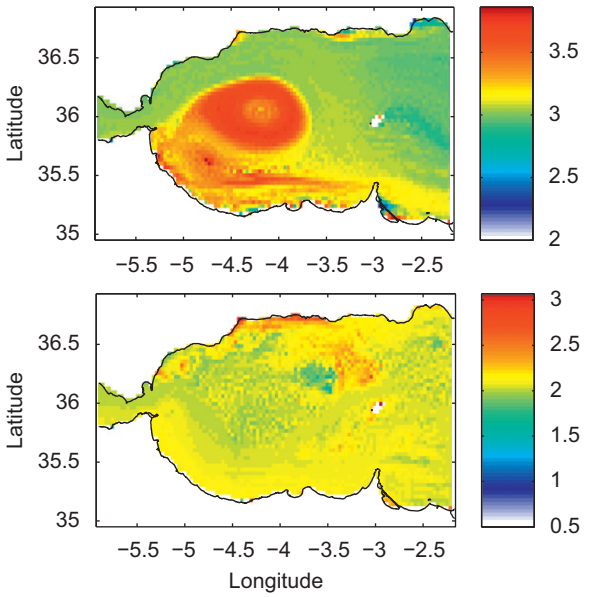

Fig. 7. Computed ^{137}Cs concentrations in unfiltered water (Bq/m^3) in the upper and lower water layers (up and down, respectively) of the AS.

passive tracers neglecting the role of sediments and suspended matter (Elbaz-Poulichet et al., 2001; Beckers et al., 2007). The first authors use a model to estimate the dilution of a conservative tracer released by the Odiel-Tinto rivers. Beckers et al. (2007) apply a numerical model to reproduce observed metal (again considering metals as passive tracers) concentrations in surface waters of the northern GoC.

Metal concentrations in the dissolved phase have been defined at the three main sources: Guadalquivir, Guadiana and Odiel-Tinto estuaries. Values are given in Beckers et al. (2007). Kinetic rates for each metal are deduced from the corresponding equilibrium k_d (IAEA, 2004) following the method described in detail in Periáñez (2005a).

The concentrations of several metals have been measured in the fine sediment fraction (<63 μm) along the Spanish coast from the Guadiana to the Guadalquivir mouths (Sainz and Ruiz, 2006; Morillo et al., 2004) and also at some points closer to the Strait of Gibraltar (Riba et al., 2002). Samples were collected at an approximate distance of 500 m from the shoreline. A comparison of measured (points) and computed (lines) metal concentrations along the northern coast of the model domain can be seen in Fig. 8. In general, there is a good agreement between the measured and calculated concentrations. Metal concentrations are very low westward from the Guadiana River. There is an increase in concentrations here since, as has already been mentioned, the three rivers drain the Iberian Pyrite Belt. Maximum concentrations exist in the mouth of the Odiel-Tinto rivers. Although river flows are much smaller than those of the Guadiana and Guadalquivir, the Odiel-Tinto rivers are considerably more contaminated (Gonzalez et al., 2007) and, indeed, they have been recognized as the main source of metals along the coast (Morillo et al., 2004).

A map of computed dissolved Zn concentrations at the surface for summer 1997 is presented in Fig. 9 together with a contour plot obtained from empirical data (Achterberg et al., 1999), which shows essentially the same banded structure. It may be clearly seen that the impacts from river outflow are restricted to a narrow band along the shore. Samples were not collected in the coastal area from Cadiz to the Strait, thus the impact is apparently restricted (in the case of observations) in Fig. 9 to the zone located to the north of Cadiz. The highest concentrations are obtained in the mouth of the Odiel-Tinto rivers, obviously as in the case of

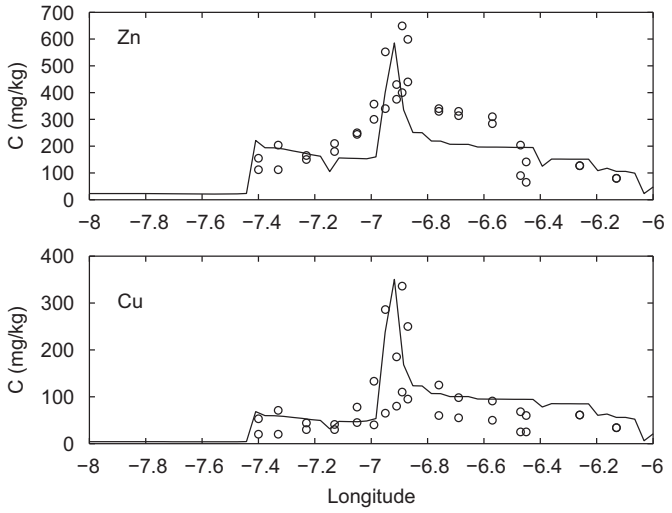

Fig. 8. Measured (circles) and computed (lines) metal concentrations in sediments along the northern coast of the model domain. The mouths of the Guadiana, Odiel-Tinto and Guadalquivir rivers are located, respectively, at the longitudes of -7.4°, -6.9° and -6.4°.

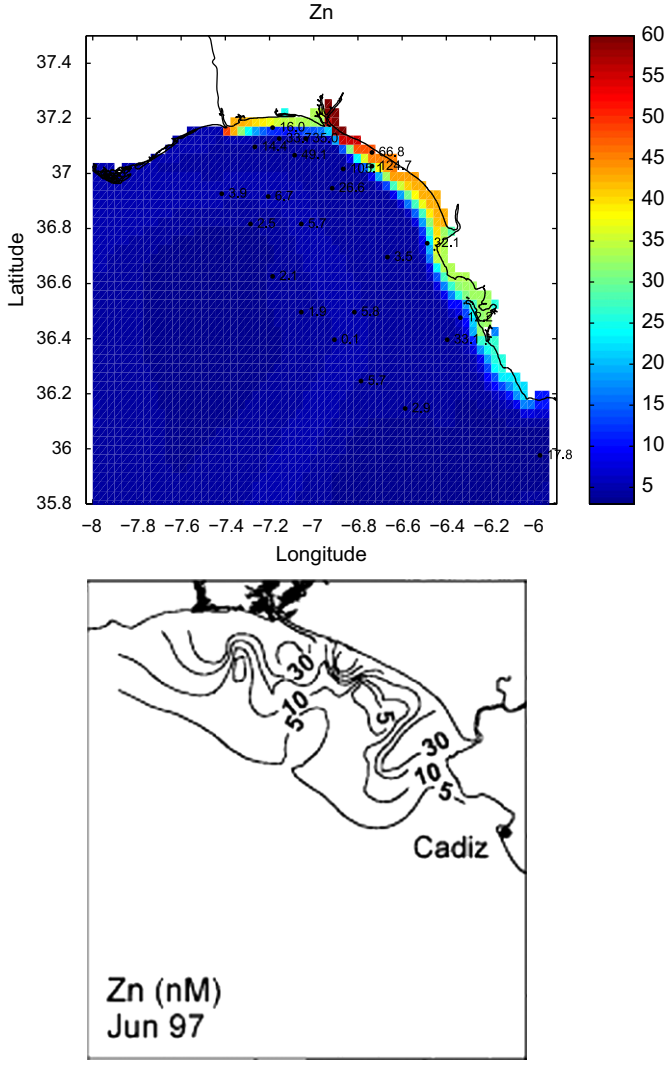

Fig. 9. Up: measured and computed (color scale) metal concentrations (nM) in surface waters of the northern GoC. Down: contour plot showing surface dissolved Zn concentrations (nM) in June 1997 from experimental data (from Achterberg et al., 1999). (For interpretation of the references to color in this figure legend, the reader is referred to the web version of this article.)

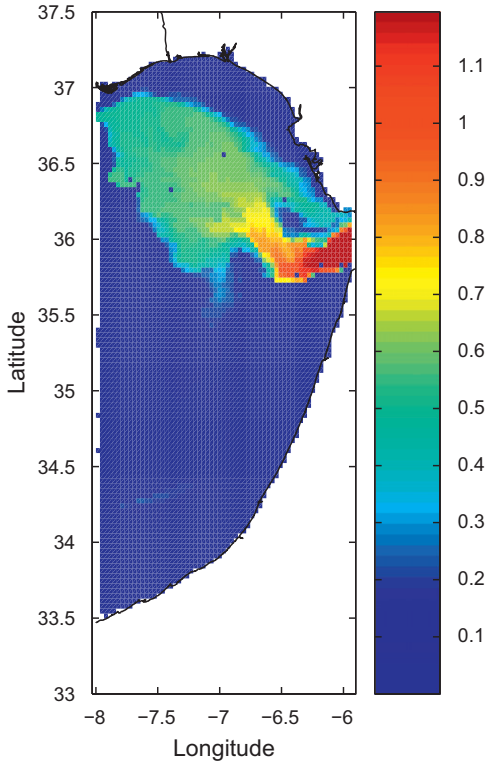

Fig. 10. Computed distribution of ^{239,240}Pu (Bq/kg) in surface bed sediments of the GoC resulting from the outflow of Mediterranean Waters.

bed sediments. The plume of dissolved metals, however, reaches the Strait of Gibraltar. Indeed, it has already been found (Elbaz-Poulichet et al., 2001) that coastal waters transport dissolved metals from the Odiel-Tinto rivers to a distance of more than 200 km. Moreover, it has been found that these rivers constitute a source of natural radionuclides into the Mediterranean through the Strait of Gibraltar (Gascó et al., 2002).

Once it seems that the model is giving a realistic representation of reactive transport in the GoC, a numerical experiment has been carried out to assess the effect of the outflow of Mediterranean Water on the Pu contamination of bed sediments in the GoC. The model is started from clean water, suspended matter and bed sediments. Pu concentration in water is specified, as a boundary condition, in the Mediterranean Water entering the GoC through the Strait of Gibraltar. Such Pu concentration is obtained from the output of the AS model (Periáñez, 2008): 0.012 Bq/m^3. The model is integrated until a steady situation is achieved. The computed Pu distribution in bed sediments is presented in Fig. 10. This results could not be compared with measurements. However, the path followed by the Mediterranean Water is clearly marked on the bed sediment as a tongue of enhanced Pu concentrations directed to the noth-west. Its shape is in agreement with the computations in Serra et al. (2005), Fig. 4b in their paper, for salinity.

4. Particle-tracking rapid-response models

4.1. Description

Particle-tracking dispersion models for dissolved contaminants and oil spills have already been described for the Strait of Gibraltar (Periáñez and Pascual-Granged, 2008) and the AS (Periáñez, 2006). However, due to the hydrodynamic models used to obtain the water circulation in such cases (a 2D model for the Strait of Gibraltar and a reduced-gravity model in the case of the AS) only pollutant releases

occurring at the sea surface could be simulated. Now, particle-tracking models have been improved and releases at any depth may be considered. This is particularly interesting, for instance, to simulate a radioactive spill from a sinking nuclear submarine.

The adsorption of pollutants by suspended and bottom sediments can also be simulated with a particle-tracking model (Periáñez and Elliott, 2002). However, these processes are neglected in the present study since suspended matter concentrations are very low in most of the GoC (Palanques et al., 1986-1987) and AS (León-Vintró et al., 1999).

Essentially, a pollutant discharge is simulated by a number of discrete, passive, particles, each one equivalent to a number of units (for instance kg). The path followed by each particle is computed, turbulent diffusion being modelled as a 3D random walk process. The density of particles per water volume unit is finally computed to obtain pollutant concentrations over the domain at the desired time and depth. Both instantaneous and continuous releases of particles can be simulated.

Advection is computed solving the following equation for each particle:

$$\frac{d\mathbf{r}}{dt} = \mathbf{q} \tag{1}$$

where $\mathbf{r}$ is the position vector of the particle and $\mathbf{q}$ is the current vector (due to wind, tide and residual circulation) at the particle position and depth, solved in components u and v.

The maximum size of the horizontal step given by the particle due to turbulence, D_h, is

$$D_h = \sqrt{12A\Delta t} \tag{2}$$

in the direction $\theta = 2\pi RAN$, where RAN is a random number between 0 and 1. This equation gives the maximum size of the step. In practice, it is multiplied by RAN to obtain the real size at a given time and for a given particle. Similarly, the maximum size of the vertical step is

$$D_v = \sqrt{2K\Delta t} \tag{3}$$

given either towards the sea surface or the sea bottom. A and K are the horizontal and vertical diffusion coefficients, respectively, as denoted in Appendix, and Δt is time step.

The horizontal diffusion coefficient depends on the horizontal grid spacing (Dick and Schonfeld, 1996). The present grid resolution gives $A = 2.0\ m^2/s$. In the case of the vertical diffusion coefficient, a typical value of $0.001\ m^2/s$ is used (Elliott et al., 2001; Dick and Schonfeld, 1996). Diffusion through the pycnocline in the AS 2-layer domain was fixed as $1.0 \times 10^{-5}\ m^2/s$ (Periáñez, 2008).

The effect of wind is included as usual in particle-tracking models. Thus, it is assumed that the water surface moves in the direction of wind at a speed equal to 3% of the wind speed 10 m above the sea surface. This current decreases logarithmically to zero at a depth usually taken as 20 m. Changing wind fields may be specified as in Periáñez and Pascual-Granged (2008).

Date and time of the discharge (and duration in the case of continuous releases) must be specified since the fate of the release will depend on the tidal state when it took place. Thus, the appropriate phase of each tidal constituent at $t = 0$ must be specified. The values used correspond to the origin of time being January 1, 2003 at 0:15 h Greenwich time.

More details about the practical aspects of the computation may be seen elsewhere (Periáñez, 2005a; Periáñez and Pascual-Granged, 2008). A summary of equations describing specific processes for radioactive and oil spills is given in Appendix D.

The model output consists of 12 snapshots at constant intervals during the simulation to show the evolution of the contamination patch over time. These snapshots can be drawn in a 3D form, or as projections on the xy, xz and yz planes. Pollutant concentration maps at any depth are obtained from the density of particles per water volume unit.

4.2. Results

Fortunately, accidents suitable for testing the particle-tracking models have not occurred in the region. Thus, some examples of results concerning hypothetical accidents are presented. Nevertheless, the dispersion of metals (in the GoC) and of fallout radionuclides (in the AS) has been satisfactorily simulated with the currents provided by the corresponding hydrodynamic models. Consequently, there is some confidence on particle-tracking model results since we must also take into account that this technique does not introduce numerical dispersion and is more suitable than finite differences to simulate situations when high contamination gradients are involved (Periáñez and Elliott, 2002).

Mean currents in AS and GoC are affected by factors as for instance atmospheric pressure differences between the Atlantic and the western Mediterranean, and thus presents some variability. Consequently, a factor which acts as a modulator of the residual current amplitude has been introduced. If 1 is used, the residual current for the mean conditions is used in the calculations. These mean currents may be amplified or reduced by specifying values for the modulator larger or smaller than 1, respectively. It is worth commenting that it is difficult to provide a value for this modulator: let us imagine that an accident occurs just now. How do we run the model? It is recommended to carry out calculations under the most probable conditions in a first guess (using the mean current, with a modulator equal to 1). Additional simulations may then be carried out using other current modulators to increase and reduce water velocities. This

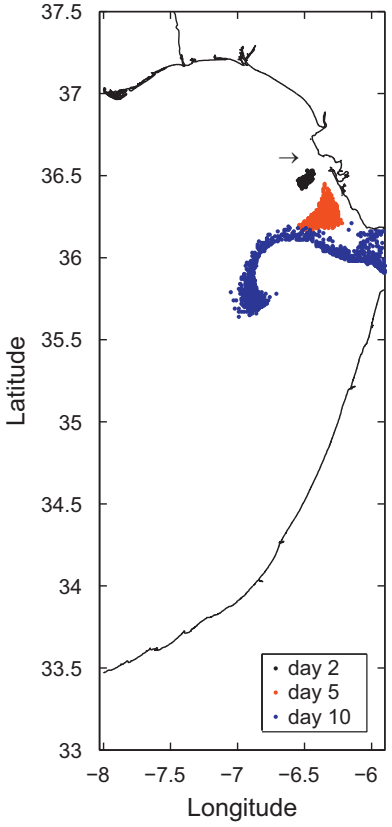

Fig. 11. Position of particles 2, 5 and 10 days after an instantaneous surface chemical spill occurring at the arrow position.

method will, at least, allow to estimate if there is any chance that a given sensitive point (a coastal town for instance) is affected by contamination. Given the short running times of the model (approximately 1.5 s per day of simulation on a Pentium 4 PC in the case of an instantaneous release), this is not a problem. This procedure has already been suggested for surface radioactive spill models recently developed for the Alboran Sea (Periáñez, 2006) and the Strait of Gibraltar (Periáñez and Pascual-Granged, 2008).

The first numerical experiment consisted of a dissolved chemical spill in front of the Bay of Cadiz (GoC). The spill was an instantaneous release at the surface on January 1, 2008 at 0:00 h (this date and time was taken just as an example) and with no wind. Snapshots showing the position of particles 2, 5 and 10 days after the accident may be seen in Fig. 11. These snapshots are projections of the 3D particle positions on the *xy* plain. The contamination patch is transported towards the Strait of Gibraltar by the residual current, although some is directed to the west by the gyre existing in front of the Strait (Fig. 3). A significant fraction of the spill has entered the Mediterranean through the Strait after 12 days.

A second experiment consisted of a long-live radionuclide release from a sunken nuclear submarine in front of Gibraltar (coordinates -5.27°, 36.10°). The release is assumed to be instantaneous (total amount 1.0×10^{12} Bq) and to occur just over the seabed (water depth 500 m at this point). The accidental release takes place at the same date and time as before and again no wind is considered. Some examples of results are presented in Fig. 12. Two maps showing radionuclide concentrations 12 days after the accident in the surface and bottom water layers are presented in Fig. 12a and b, respectively. In the bottom water layer the current is directed to the west and, consequently, most of the radionuclides move in this direction. Nevertheless, some of them cross the pycnocline (the interface separating both water layers) and reach the surface water layer, which moves to the east (see Fig. 2). Thus, a fraction of the release is transported to the east along the Spanish coast. Later this radionuclide patch is deflected to the south by the Western Alboran Gyre. A projection of particle positions 12 days after the accident on the *xz* plane is presented in Fig. 12c. The pycnocline depth in the AS is in the range of approximately 170–220 m. It acts as a natural barrier for mixing and, indeed, only a small fraction of the release crosses it, as it may be seen comparing the color scales in Fig. 12. Water depths in the Strait of Gibraltar decrease very fast from about -5.5° towards the west. Most of the patch is trapped in this abrupt slope (see Fig. 12c). Also, it is in this region of abrupt topography where mixing through the pycnocline mainly occurs. Experiments in other parts of the AS, concerning releases at the same depth, have not shown any significant mixing through the interface.

5. Conclusions

Pollutant dispersion processes in the Gulf of Cadiz and Alboran Sea have been studied through numerical modelling. Two kind of dispersion models have been developed: finite difference and

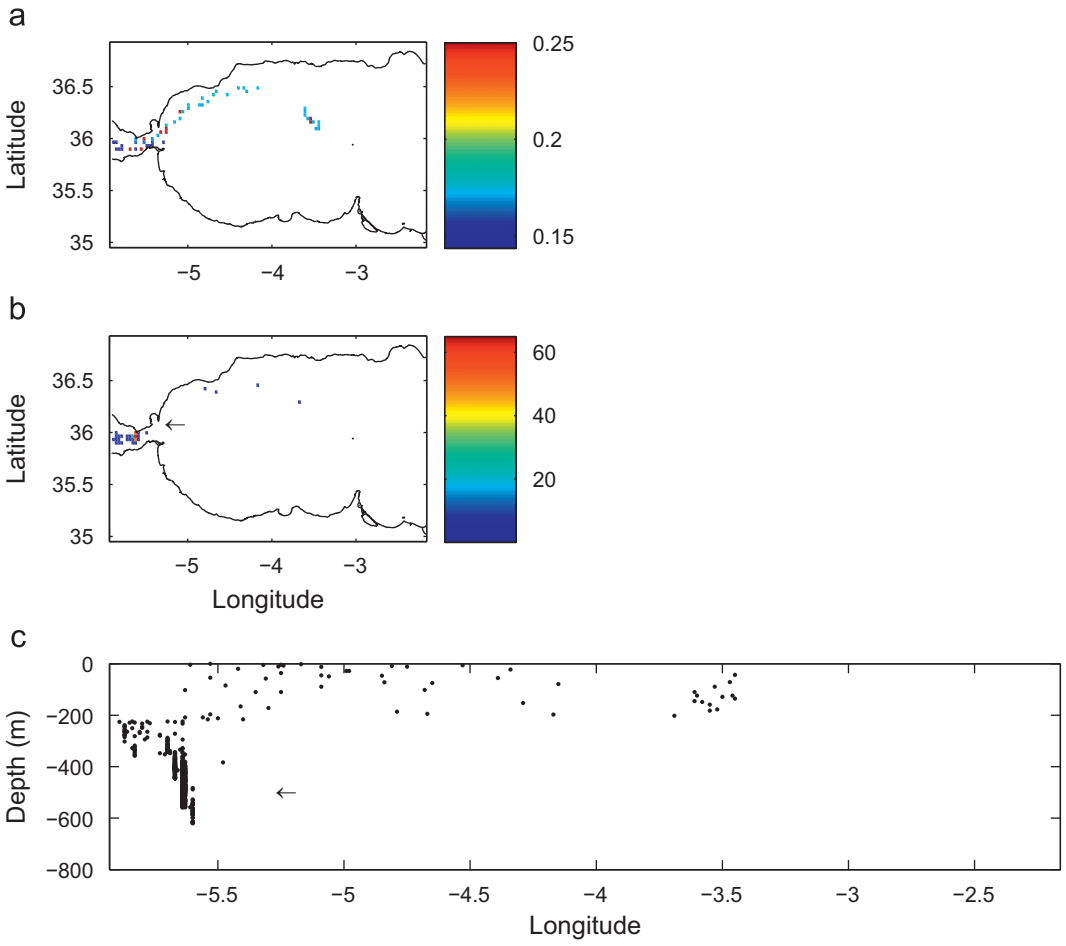

Fig. 12. Radionuclide concentrations (Bq/m^3) in the upper (a) and lower (b) water layers of the AS 12 days after the release (see text). (c) Projection of particle positions on the *xz* plane. The position of the release is indicated by the arrow in panels (b) and (c). (For interpretation of the references to color in this figure legend, the reader is referred to the web version of this article.)

rapid-response Lagrangian models. Water circulation, required to solve dispersion, is obtained from appropriate hydrodynamic models for each domain. These models have been tested by means of comparisons of computed tides and currents with measurements in the GoC and the AS.

The finite difference dispersion models include water–sediment interactions. In the Alboran Sea, this model has been applied to simulate the dispersion of fallout radionuclides. Computed ^{137}Cs and ^{239,240}Pu concentrations in bed sediments and the water column have been compared with observations. In the case of the Gulf of Cadiz, the contamination of bed sediments by metals discharged by the main rivers draining the southern Iberian Peninsula has been adequately reproduced. The impact from river outflow is restricted to a narrow band along the shore, the area of the Odiel-Tinto river mouth being the more contaminated. The plume of dissolved metals reaches the Strait of Gibraltar confirming that coastal waters transport dissolved metals from the Odiel-Tinto rivers to a distance of more than 200 km and that these rivers may constitute a source of metals and radionuclides into the Mediterranean through the Strait of Gibraltar.

The dispersion of Pu entering the Gulf of Cadiz with the outflow of Mediterranean Water has been simulated with the model. The path followed by the Mediterranean Water is clearly marked on the bed sediment as a tongue of enhanced Pu concentrations. Its shape is in agreement with earlier salinity computations.

Results of the finite difference dispersion models provide an extra validation of the water circulation obtained from the hydrodynamic models. Then, water circulation is used in rapid-response particle-tracking dispersion models, which are appropriate tools to support the decision-making process after an emergency situation. Although results of these models could not be compared with observations, two examples concerning hypothetical accidents have been presented and discussed. These numerical experiments, moreover, are useful to improve our knowledge about processes occurring in the environment. For instance, it has been found that mixing of contaminants through the pycnocline in the Alboran Sea essentially occurs in the area of abrupt topography change of the Strait of Gibraltar.

Acknowledgment

The author is indebted to the Agencia Española de Cooperación Internacional for partially funding this work, and to the Spanish Ministerio de Educación y Ciencia for a fellowship to stay during three months at the University of Wales, Bangor, where part of this work was carried out.

Appendix A. Hydrodynamic models

A.1. 2D barotropic model

The 2D-depth averaged model used to compute tides is based on the following equations:

$$\frac{\partial \zeta}{\partial t}+\frac{\partial}{\partial x}(Hu)+\frac{\partial}{\partial y}(Hv)=0 \tag{4}$$

$$\frac{\partial u}{\partial t}+u\frac{\partial u}{\partial x}+v\frac{\partial u}{\partial y}+g\frac{\partial \zeta}{\partial x}-\Omega v+\frac{\tau_u}{\rho_w H}=A\left(\frac{\partial^2 u}{\partial x^2}+\frac{\partial^2 u}{\partial y^2}\right) \tag{5}$$

$$\frac{\partial v}{\partial t}+u\frac{\partial v}{\partial x}+v\frac{\partial v}{\partial y}+g\frac{\partial \zeta}{\partial y}+\Omega u+\frac{\tau_v}{\rho_w H}=A\left(\frac{\partial^2 v}{\partial x^2}+\frac{\partial^2 v}{\partial y^2}\right) \tag{6}$$

where u and v are the depth averaged water velocities along the x- and y-axes, h is the depth of water below the mean sea level, ζ is the displacement of the water surface above the mean sea level measured upwards, $H=h+\zeta$ is the total water depth, Ω is the Coriolis parameter ($\Omega=2w\sin\beta$, where w is the Earth rotational angular velocity and β is latitude), g is acceleration due to gravity, ρ_w is water density and A is the horizontal eddy viscosity. τ_u and τ_v are friction stresses that have been written in terms of a quadratic law:

$$\tau_u=k\rho_w u\sqrt{u^2+v^2}$$

$$\tau_v=k\rho_w v\sqrt{u^2+v^2} \tag{7}$$

where k is the bed friction coefficient.

A.2. 3D baroclinic model

The full 3D hydrodynamic equations including the terms corresponding to density gradients are written in the hydrostatic and Boussinesq approximations as

$$\frac{\partial \zeta}{\partial t}+\frac{\partial}{\partial x}\left[(h+\zeta)\int_{-h}^{\zeta}u\,dz\right]+\frac{\partial}{\partial y}\left[(h+\zeta)\int_{-h}^{\zeta}v\,dz\right]=0 \tag{8}$$

$$\frac{\partial u}{\partial t}+u\frac{\partial u}{\partial x}+v\frac{\partial u}{\partial y}-\Omega v+g\frac{\partial \zeta}{\partial x}+\frac{g}{\rho_0}\int_z^{\zeta}\frac{\partial \rho_w}{\partial x}\,dz = \frac{\partial}{\partial z}\left(K\frac{\partial u}{\partial z}\right)+A\left(\frac{\partial^2 u}{\partial x^2}+\frac{\partial^2 u}{\partial y^2}\right) \tag{9}$$

$$\frac{\partial v}{\partial t}+u\frac{\partial v}{\partial x}+v\frac{\partial v}{\partial y}+\Omega u+g\frac{\partial \zeta}{\partial y}+\frac{g}{\rho_0}\int_z^{\zeta}\frac{\partial \rho_w}{\partial y}\,dz = \frac{\partial}{\partial z}\left(K\frac{\partial v}{\partial z}\right)+A\left(\frac{\partial^2 v}{\partial x^2}+\frac{\partial^2 v}{\partial y^2}\right) \tag{10}$$

where ρ_w is water density, ρ_0 is a reference density, and K and A are the vertical and horizontal eddy viscosities, respectively.

The vertical component of the water velocity, w, is obtained from the continuity equation:

$$\frac{\partial u}{\partial x}+\frac{\partial v}{\partial y}+\frac{\partial w}{\partial z}=0 \tag{11}$$

The water density is derived from a equation of state relating density to salinity and temperature:

$$\rho_w=\rho_0[1-\alpha(T-T_0)+\beta(S-S_0)] \tag{12}$$

where S is salinity, T is temperature, $\alpha=2.41\times10^{-4}$ and $\beta=7.45\times10^{-4}$. The reference salinity is taken as $\rho_0=999.7$ kg/m^3 at $S_0=0$ and $T_0=10$ °C.

Water salinity is determined from an advection–diffusion equation:

$$\frac{\partial S}{\partial t}+u\frac{\partial S}{\partial x}+v\frac{\partial S}{\partial y}+w\frac{\partial S}{\partial z}=A\left(\frac{\partial^2 S}{\partial x^2}+\frac{\partial^2 S}{\partial y^2}\right)+\frac{\partial}{\partial z}\left(K\frac{\partial S}{\partial z}\right) \tag{13}$$

and a similar equation is used for temperature:

$$\frac{\partial T}{\partial t}+u\frac{\partial T}{\partial x}+v\frac{\partial T}{\partial y}+w\frac{\partial T}{\partial z}=A\left(\frac{\partial^2 T}{\partial x^2}+\frac{\partial^2 T}{\partial y^2}\right)+\frac{\partial}{\partial z}\left(K\frac{\partial T}{\partial z}\right) \tag{14}$$

Vertical eddy viscosity is determined from a 1-equation turbulence model. The equation for the turbulent kinetic energy E is

$$\frac{\partial E}{\partial t}=K\left\{\left(\frac{\partial u}{\partial z}\right)^2+\left(\frac{\partial v}{\partial z}\right)^2\right\}+\beta_0\frac{\partial}{\partial z}\left(K\frac{\partial E}{\partial z}\right)-\varepsilon+\frac{g}{\rho_0}K\frac{\partial \rho}{\partial z} \tag{15}$$

The first term in the right side of the equation represents generation of turbulence by the vertical shear, the second term is diffusion of turbulence and the last term is loss of turbulence by buoyancy (conversion of kinetic energy into potential energy).

ε represents dissipation of turbulence that is written as

$$\varepsilon = C_1 E^{3/2}\ell \tag{16}$$

where ℓ is a mixing length and C_1 is a numeric coefficient. The vertical viscosity is finally written as a function of energy as

$$K = C_0 \ell E^{1/2} + \lambda_t \tag{17}$$

where C_0 is a numeric coefficient and λ_t is a background value of viscosity that is the minimum possible value that it may have. The values of the numeric constants appearing above are $\beta_0 = 0.73$, $C_0 = C^{1/4}$, $C_1 = C_0^3$ and $C = 0.046$. The background viscosity is fixed as $\lambda_t = 10^{-4}$ m^2/s.

The mixing length is derived from an algebraic expression:

$$\ell = \frac{1}{1/\ell_1 + 1/\ell_2} \tag{18}$$

with

$$\ell_1 = \kappa(z + z_0 + h)e^{\beta_1(z+h)/h} \tag{19}$$

$$\ell_2 = \kappa(z_s - z) \tag{20}$$

where $\kappa = 0.4$ is the von Karman's constant, $\beta_1 = -2.0$ and z_s and z_0 are the roughness lengths of the sea surface and bottom, respectively.

A.3. 2-layer model

Two water layers with different densities are flowing in opposite directions in the Alborán Sea. The equations describing this flow are the following (in the vector formulation of Izquierdo et al., 2001):

$$\frac{\partial(H_1\vec{u_1})}{\partial t} + \nabla(H_1\vec{u_1}\cdot\vec{u_1}) + \Omega\vec{k} \times H_1\vec{u_1} + gH_1\nabla\zeta_1 = -\vec{\tau_1}/\rho_1 + AH_1\nabla^2\vec{u_1} \tag{21}$$

$$\frac{\partial H_1}{\partial t} + \nabla\cdot H_1\vec{u_1} = 0 \tag{22}$$

$$\frac{\partial(H_2\vec{u_2})}{\partial t} + \nabla(H_2\vec{u_2}\cdot\vec{u_2}) + \Omega\vec{k} \times H_2\vec{u_2} + g\frac{\rho_1}{\rho_2}H_2\nabla\zeta_1 + g'H_2\nabla\zeta_2 = (\vec{\tau_1} - \vec{\tau_2})/\rho_2 + AH_2\nabla^2\vec{u_2} \tag{23}$$

$$\frac{\partial H_2}{\partial t} + \nabla\cdot H_2\vec{u_2} = 0 \tag{24}$$

with indexes 1 and 2 for the upper and lower layers, respectively. In these equations H_i is the thickness of the water layer, ρ_i is water density in each layer, A is a horizontal friction coefficient and g' is the reduced gravity:

$$g' = g\frac{\rho_2 - \rho_1}{\rho_2} \tag{25}$$

ζ_1 is the elevation of the sea surface with respect to the mean level and ζ_2 is the depth of the interface between layers. Finally $\vec{\tau_1}$ and $\vec{\tau_2}$ are friction stresses between water layers and between the lower layer and the seabed, respectively. They are formulated in terms of a quadratic law as usual:

$$\vec{\tau_1} = c_1\rho_1|\vec{u_1} - \vec{u_2}|(\vec{u_1} - \vec{u_2})$$

$$\vec{\tau_2} = c_2\rho_2|\vec{u_2}|\vec{u_2} \tag{26}$$

where c_1 and c_2 are the interfacial and bottom friction coefficients.

Appendix B. Suspended matter transport

The equation which provides the suspended matter concentration, m, is

$$\frac{\partial m}{\partial t} + u\frac{\partial m}{\partial x} + v\frac{\partial m}{\partial y} + (w - w_s)\frac{\partial m}{\partial z} = A\left(\frac{\partial^2 m}{\partial x^2} + \frac{\partial^2 m}{\partial y^2}\right) + \frac{\partial}{\partial z}\left(K\frac{\partial m}{\partial z}\right) \tag{27}$$

where w_s is the settling velocity of suspended particles. The deposition and erosion terms are incorporated into the seabed boundary condition of the equation. The deposition rate is written as

$$DP = w_s m(b)\left(1 - \frac{\tau_b}{\tau_{cd}}\right) \tag{28}$$

where $m(b)$ is particle concentration evaluated at the sea bottom, τ_b is bottom stress due to tides and the residual current, and τ_{cd} is a critical deposition stress above which no deposition occurs since particles are maintained in suspension by water turbulence.

The settling velocity is determined from Stokes's law:

$$w_s = \frac{\rho - \rho_w}{\rho_w}\frac{gD^2}{18v} \tag{29}$$

where ρ and D are suspended particle density and diameter, respectively, and v is kinematic viscosity of water. The erosion rate is written in terms of the erodability constant:

$$ER = Ef\left(\frac{\tau_b}{\tau_{ce}} - 1\right) \tag{30}$$

where E is the erodability constant, f gives the fraction of fine particles in the bed sediment and τ_{ce} is a critical erosion stress below which no erosion occurs. The model can also calculate sedimentation rates (SR) as the balance between the deposition and erosion terms.

Appendix C. Finite difference transport equations

The migration of pollutants to the deep sediment is treated as a decay process with constant λ_{burial} given by

$$\lambda_{burial} = \frac{\mathrm{SR}}{\rho_s L} \tag{31}$$

where L is the sediment mixing depth (the distance to which the dissolved phase penetrates the sediment) and ρ_s is the sediment bulk density (dry mass divided by wet volume).

It is known that adsorption depends on the surface of particles per water volume unit at each point and time. This quantity has been denoted as the exchange surface. Thus, the kinetic coefficient $k_{1,k}$ is written as

$$k_{1,k} = \chi(S_{m,k} + S_s\delta_{k,2}) = k_{1,k}^m + k_1^s \tag{32}$$

where S_m and S_s are the exchange surfaces for suspended matter and bottom sediments, respectively (dimensions $[L]^{-1}$) and χ is a parameter with the dimensions of a velocity denoted as the exchange velocity. The index $k = 1,2$ represents each water layer (surface and bottom, respectively). The delta function is introduced to take into account that only the bottom layer interacts with the bed sediment.

Assuming spherical particles, the exchange surfaces are written as

$$S_{m,k} = \frac{3m_k}{\rho R} \tag{33}$$

and

$$S_s = \frac{3Lf\phi(1-p)}{RH_2} \tag{34}$$

where R and ρ are particle radius and density, respectively, m_k is the suspended matter concentration in layer k, f is the fraction of small particles in the sediment, p is sediment porosity and ϕ is a correction factor that takes into account that part of the sediment particle surface may be hidden by other sediment particles. Finally, H_2 is the thickness of the bottom water layer. The kinetic coefficient k_2 is considered to be constant.

The equation that gives the time evolution of the pollutant concentration in the dissolved phase, C_d, is

$$\frac{\partial(HC_d)_k}{\partial t}+\frac{\partial(uHC_d)_k}{\partial x}+\frac{\partial(vHC_d)_k}{\partial y}=\frac{\partial}{\partial x}\left(H_kA\frac{\partial C_{d,k}}{\partial x}\right)+\frac{\partial}{\partial y}\left(H_kA\frac{\partial C_{d,k}}{\partial y}\right)+\frac{\partial}{\partial z}(KC_{d,k})-k^m_{1,k}H_kC_{d,k}+k_2H_km_kC_{s,k}-k^s_1H_2C_{d,2}+\delta_{k,2}k_2A_sL\rho_sf\phi-\lambda H_kC_{d,k} \quad (35)$$

where C_s and A_s are pollutant concentrations in suspended matter and the bed sediment mixed layer, respectively, and λ is a decay constant (for instance radioactive).

The equation for the time evolution of pollutant concentration in suspended matter is

$$\frac{\partial(HC_sm)_k}{\partial t}+\frac{\partial(uHC_sm)_k}{\partial x}+\frac{\partial(vHC_sm)_k}{\partial y}=\frac{\partial}{\partial x}\left(H_kA\frac{\partial(C_sm)_k}{\partial x}\right)+\frac{\partial}{\partial y}\left(H_kA\frac{\partial(C_sm)_k}{\partial y}\right)+\frac{\partial}{\partial z}(KC_{s,k}m_k)-w_{s,1}m_1C_{s,1}(\delta_{k,1}-\delta_{k,2})+k^m_{1,k}C_{d,k}-k_2m_kC_{s,k}-\delta_{k,2}\mathrm{SR}C_{s,k}-\lambda H_km_kC_{s,k} \quad (36)$$

where w_s is particle settling velocity. Finally, for the bed sediment pollutant concentration we have

$$\frac{\partial A_s}{\partial t}=k^s_1\frac{H_2C_{d,2}}{\rho_sLf}-k_2A_s\phi+\mathrm{SR}\frac{C_{s,2}}{\rho_sLf}-(\lambda+\lambda_{burial})A_s \quad (37)$$

in the mixed sediment depth. The total contaminant content, A_p, in the sediment below the mixed depth is given by the following equation:

$$\frac{\partial A_p}{\partial t}=\lambda_{burial}\rho_sLfA_s-\lambda A_p \quad (38)$$

The contaminant concentration in the sediment mixed depth is given by fA_s. This is what would be obtained from a surface sediment sample where a coarse sediment fraction $(1-f)$ exists with negligible pollutant concentration.

Appendix D. Particle-tracking dispersion processes

Radioactive decay can be treated using a stochastic method if it is assumed that the probability p of removal of a particle at each time step is

$$p=1-e^{-\lambda\Delta t} \quad (39)$$

where λ is the radioactive decay constant. In practice, a random number is generated for each particle at each time step. If $RAN\le p$ then the particle is removed from the computation. Obviously, in the case of a stable chemical pollutant $\lambda=0$.

In the case of oil spills the buoyancy force depends on the density and size of droplets. The vertical velocity, w, can be described as (Proctor et al., 1994; Korotenko et al., 2004):

$$w=\frac{gd^2(1-\rho_0/\rho_w)}{18\nu} \quad (40)$$

for small droplets with diameter $d\le d_c$ (laminar motion). In this equation ρ_w and ρ_0 are the densities of water and oil, respectively, and ν is the water kinematic viscosity. For large droplets with $d>d_c$ (turbulent motion) the vertical velocity is

$$w=\left(\tfrac{8}{3}gd(1-\rho_0/\rho_w)\right)^{1/2} \quad (41)$$

The critical diameter, d_c, is given by the expression

$$d_c=\frac{9.52\nu^{2/3}}{g^{1/3}(1-\rho_0/\rho_w)^{1/3}} \quad (42)$$

that is deduced matching the Reynolds numbers at which the transition from laminar to turbulent flow occurs.

The diameter of each oil droplet in the simulation is assigned randomly between a minimum and maximum diameter, $d_{min}-d_{max}$.

The effects of oil evaporation and decomposition are treated in a similar way as radioactive decay using e-folding times (Proctor et al., 1994). Thus, the probability of removal of particle in a time step is given by Eq. (39). The decay constant is related to the e-folding time by $\lambda=1/T_e$. Different e-folding times are used for evaporation, T_{ev}, and decomposition, T_{de}. Additionally, only particles within a depth z_{ev} m below the surface can be evaporated, whereas droplets at any depth can experience decomposition. If during a computation an oil droplet reaches the coastline, it is considered *beached*. Thus, the droplet stays in the coast without moving any more. In the case of a chemical or radioactive spill particles are simply reflected at the coastline. Particles which leave the model domain through an open boundary are removed from the computation.

References

Achterberg, E.P., Braungardt, C., Morley, N.H., Elbaz-Poulichet, F., Leblanc, M., 1999. Impact of Los Frailes mine spill on riverine, estuarine and coastal waters in southern Spain. Water Res. 33, 3387–3394.

Ambar, I., Howe, M.R., 1979. Observations of the Mediterranean outflow. 2, the deep circulation in the vicinity of the Gulf of Cadiz. Deep Sea Res. 26A, 555–568.

Beckers, J.M., Achterberg, E.P., Braungardt, C., 2007. Comparison of high spatial resolution trace metal distributions with model simulations for surface waters of the Gulf of Cadiz. Estuarine Coastal Shelf Sci. 74, 599–609.

Cancino, L., Neves, R., 1999. Hydrodynamic and sediment suspension modelling in estuarine systems. Part I: description of the numerical models. J. Mar. Syst. 22, 105–116.

Criado-Aldeanueva, F., García-Lafuente, J., Vargas, J.M., del Río, J., Vázquez, A., Reul, A., Sánchez, A., 2006. Distribution and circulation of water masses in the Gulf of Cadiz from in situ observations. Deep Sea Res. II 53, 1144–1160.

Dick, S., Schonfeld, W., 1996. Water transport and mixing in the North Frisian Wadden Sea. Results of numerical investigations. Ger. J. Hydrogr. 48, 27–48.

Dyke, P.P.G., 2001. Coastal and Shelf Sea Modelling. Kluwer, The Netherlands.

Echevarría, F., García-Lafuente, J., Bruno, M., Gorsky, G., Goutx, M., González, N., García, C.M., Gómez, F., Vargas, J.M., Picheral, M., Striby, L., Varela, M., Alonso, J.J., Reul, A., Cozar, A., Prieto, L., Sarhan, T., Plaza, F., Jiménez-Gómez, F., 2002. Physical-biological coupling in the Strait of Gibraltar. Deep Sea Res. II 49, 4115–4130.

Elbaz-Poulichet, F., Morley, N.H., Beckers, J.M., Nomerange, P., 2001. Metal fluxes through the Strait of Gibraltar: the influence of the Odiel and Tinto Rivers (SW Spain). Mar. Chem. 73, 193–213.

Elliott, A.J., Wilkins, B.T., Mansfield, P., 2001. On the disposal of contaminated milk in coastal waters. Mar. Pollut. Bull. 42, 927–934.

García-Lafuente, J., Delgado, J., Criado-Aldeanueva, F., Bruno, M., del Río, J., Vargas, J.M., 2006. Water mass circulation on the continental shelf of the Gulf of Cadiz. Deep Sea Res. II 53, 1182–1197.

Gascó, C., Antón, M.P., Delfanti, R., González, A.M., Meral, J., Pappuci, C., 2002. Variation of the activity concentrations and fluxes of natural (^{210}Po, ^{210}Pb) and anthropogenic (^{239,240}Pu, ^{137}Cs) radionuclides in the Strait of Gibraltar (Spain). J. Environ. Radioact. 62, 241–262.

Gonzalez, R., Araujo, M.F., Burdloff, D., Cachao, M., Cascalho, J., Corredeira, C., Dias, J.M.A., Fradique, C., Ferreira, J., Gomes, C., Machado, A., Mendes, I., Rocha, F., 2007. Sediment and pollutant transport in the northern Gulf of Cadiz: a multi-proxy approach. J. Mar. Syst. 68, 1–23.

Heburn, G.W., La Violette, P., 1990. Variations in the structure of the anticyclonic gyres found in the Alborán Sea. J. Geophys. Res. 95C2, 1599–1613.

IAEA, 2004. Sediment Distribution Coefficients and Concentration Factors for Biota in the Marine Environment. Technical Reports Series 422, Vienna.

Ivanovich, M., Harmon, R.S., 1992. Uranium-series Disequilibrium: Applications to Earth, Marine and Environmental Sciences. Clarendon Press, Oxford.

Izquierdo, A., Tejedor, L., Sein, D.V., Backhaus, J.O., Brandt, P., 2001. Control variability and internal bore evolution in the Strait of Gibraltar: a 2D two-layer model study. Estuarine Coastal Shelf Sci. 53, 637–651.

Korotenko, K.A., Mamedov, R.M., Kontar, A.E., Korotenko, L.A., 2004. Particle-tracking method in the approach for prediction of oil slick transport in the sea: modelling oil pollution resulting from river input. J. Mar. Syst. 48, 159–170.

Kowalick, Z., Murty, T.S., 1993. Numerical Modelling of Ocean Dynamics. World Scientific, Singapore.

León-Vintró, L., Mitchell, P.I., Condren, O.M., Downes, A.B., Papucci, C., Delfanti, R., 1999. Vertical and horizontal fluxes of plutonium and americium in the western Mediterranean and the Strait of Gibraltar. Sci. Total Environ. 237/238, 77–91.

Lumborg, U., Windelin, A., 2003. Hydrography and cohesive sediment modelling: application to the Romo Dyb tidal area. J. Mar. Syst. 38, 287–303.

Machín, F., Pelegrí, J.L., Marrero-Díaz, A., Laiz, I., Ratsimandresey, A.W., 2006. Near-surface circulation in the southern Gulf of Cadiz. Deep Sea Res. II 53, 1161–1181.

Mañanes, R., Bruno, M., Alonso, J., Fraguela, B., Tejedor, L., 1998. Non-linear interaction between tidal and subinertial barotropic flows in the Strait of Gibraltar. Oceanol. Acta 21, 33–46.

Masqué, P., Fabres, J., Canals, M., Sanchez-Cabeza, J.A., Sanchez-Vidal, A., Cacho, I., Calafat, A.M., Bruach, J.M., 2003. Accumulation rates of major constituents of hemipelagic sediments in the deep Alborán Sea: a centennial perspective of sedimentary dynamics. Mar. Geol. 193, 207–233.

Mellor, G.L., 2004. User Guide for a Three-dimensional, Primitive Equation, Ocean Model. Princeton University, US.

Morillo, J., Usero, J., Gracia, I., 2004. Heavy metal distribution in marine sediments from the southwest coast of Spain. Chemosphere 55, 431–442.

NOAA, 1982. Computer Applications to Tides in the National Ocean Survey. Supplement to Manual of Harmonic Analysis and Prediction of Tides (Special Publication No. 98). National Ocean Service, National Oceanic and Atmospheric Administration, U.S. Department of Commerce, January 1982.

Palanques, A., Plana, F., Maldonado, A., 1986-1987. Estudio de la materia en suspensión en el Golfo de Cádiz. Acta Geol. Hisp. 21–22, 491–497 (in Spanish).

Peliz, A., Dubert, J., Marchesielo, P., Teles-Machado, A., 2007. Surface circulation in the Gulf of Cadiz: model and mean flow structure. J. Geophys. Res. 112, C11015 20 pp.

Periáñez, R., 2004. The dispersion of ^{137}Cs and ^{239,240}Pu in the Rhone River plume: a numerical model. J. Environ. Radioact. 77, 301–324.

Periáñez, R., 2005a. Modelling the Dispersion of Radionuclides in the Marine Environment. Springer-Verlag, Heidelberg.

Periáñez, R., 2005b. Modelling the transport of suspended particulate matter by the Rhone River plume (France). Implications for pollutant dispersion. Environ. Pollut. 133, 351–364.

Periáñez, R., 2006. Modelling surface radioactive spill dispersion in the Alborán Sea. J. Environ. Radioact. 90, 48–67.

Periáñez, R., 2008. A modelling study on ^{137}Cs and ^{239,240}Pu behaviour in the Alborán Sea, western Mediterranean. J. Environ. Radioact. 99, 694–715.

Periáñez, R., Elliott, A.J., 2002. A particle-tracking method for simulating the dispersion of non-conservative radionuclides in coastal waters. J. Environ. Radioact. 58, 13–33.

Periáñez, R., Pascual-Granged, A., 2008. Modelling surface radioactive, chemical and oil spills in the Strait of Gibraltar. Comput. Geosci. 34, 163–180.

Perkins, H., Kinder, T., La Violette, P., 1990. The Atlantic inflow in the western Alborán Sea. J. Phys. Oceanogr. 20, 242–263.

Preller, R.H., 1986. A numerical model study of the Alborán Sea gyre. Prog. Oceanogr. 16, 113–146.

Proctor, R., Flather, R.A., Elliott, A.J., 1994. Modelling tides and surface drift in the Arabian Gulf: application to the Gulf oil spill. Cont. Shelf Res. 14, 531–545.

Pugh, D.T., 1987. Tides, Surges and Mean Sea Level. Wiley, Chichester.

Riba, I., Del Valls, T.A., Forja, J.M., Gómez-Parra, A., 2002. Influence of the Aznalcóllar minning spill on the vertical distribution of heavy metals in sediments from the Guadalquivir estuary (SW Spain). Mar. Pollut. Bull. 44, 39–47.

Sainz, A., Ruiz, F., 2006. Influence of the very polluted inputs of the Tinto-Odiel system on the adjacent littoral sediments of southwestern spain: a statistical approach. Chemosphere 62, 1612–1622.

Schwiderski, E.W., 1980a. Ocean tides, part 1: global ocean tidal equations. Mar. Geod. 3, 161–217.

Schwiderski, E.W., 1980b. Ocean tides, part 2: a hydrodynamical interpolation model. Mar. Geod. 3, 219–255.

Serra, N., Ambar, I., Kase, R.H., 2005. Observations and numerical modelling of the Mediterranean outflow splitting and eddy generation. Deep Sea Res. II 52, 383–408.

Tsimplis, M.N., Proctor, R., Flather, R.A., 1995. A two dimensional tidal model for the Mediterranean Sea. J. Geophys. Res. 100, 16223–16239.

Yanagi, T., 1999. Coastal Oceanography. Kluwer, The Netherlands.